IEEE Access
Multidisciplinary | Rapid Review | Open Access Journal

Received June 4, 2017, accepted July 24, 2017, date of publication August 23, 2017, date of current version September 6, 2017.

Digital Object Identifier 10.1109/ACCESS.2017.2741527

Setup for EMI Shielding Effectiveness Tests of Electrically Conductive Polymer Composites at Frequencies up to 3.0 GHz

ROSÉRIO VALENTE[1,2], CHRIS DE RUIJTER[2], DANIEL VLASVELD[2], SYBRAND VAN DER ZWAAG[1], AND PIM GROEN[1]

[1]Novel Aerospace Materials Group, Faculty of Aerospace Engineering, Delft University of Technology, 2629 HS Delft, The Netherlands
[2]Promolding B.V., 2497 GC The Hague, The Netherlands

Corresponding author: Rosério Valente (r.d.vieiravalente@tudelft.nl)

This work was supported by the European Union's Horizon 2020 Research and Innovation Program under the Marie Skłodowska Curie Grant Agreement no. 642890 (http://thelink-project.eu/).

ABSTRACT Conductive polymer composites have been receiving increased interest both from the scientific community and industry with a special focus on electromagnetic interference (EMI) shielding applications. In this paper, we present the design, EM wave simulation, and validation through S-parameters measurements of an EMI shielding effectiveness (SE) tester based on the ASTM D4935 standard, to be used in the development of such materials. EM wave simulations and computer aided design were used in parallel to improve the SE test setup performance, which resulted in a unique low-loss coaxial–spherical–conical smooth transition design that ensured the best tradeoff between sample size and performance. The proposed SE tester has an insertion loss smaller than 1 dB, with good reproducibility and a setup-independent frequency response in the frequency range from a few kHz up to 3 GHz.

INDEX TERMS ASTM D4935, coaxial sample holder, conductive polymer composites, electromagnetic interference, EMI test method, shielding effectiveness, S-parameters.

I. INTRODUCTION

Current technologies rely heavily on electronic equipment and wireless communication systems using a wide range of frequencies signals. Worldwide efforts on the development and integration of the next generation of wireless networks, the 'fifth generation' or 5G and inherent key emerging technologies [1] envision specific application domains. Concepts such as Urban Internet of Things (IoT) designed to support the Smart City vision [2], intelligent transportation and wireless sensor networks (WSN) together with more industry motivated systems such as wireless avionics intra-communication (WAIC) in the aviation, and other infrastructure systems that go in hand with the IoT and the Industry 4.0, are examples on how current technologies increasingly depend on wireless communication systems.

Technological trends such the ones seen in the wireless communications, tighter electromagnetic interference (EMI) and electrostatic discharge (ESD) regulations together with higher demands for greener solutions and the need for multi-purpose materials brings new challenges which motivates, in particular, the study of the electromagnetic interference shielding of conductive polymer composites (CPC).

Problems inherent to electromagnetic interference can be solved using different approaches such as grounding, bonding, filtering, isolating and by shielding [3]. In particular EMI shielding consists in the isolation of sensitive electronic equipment from unwanted electrical noise through the use of conductive barriers.

EMI shielding is strongly influenced by the design of the enclosure serving as shield, mounting of the enclosure, gaskets used, environmental exposure, continuity of the shield [4], among others, and ultimately by the material used to build the part serving as the EMI shield.

In the context of polymer nanocomposites factors such as the small scale of the fillers, the polymer-filler affinity, and the thermo-mechanical history involved on the composite processing chain that dictates the filler dispersion, distribution and filler orientation, makes the prediction of the electrical properties on such materials a very challenging task. Therefore, in contrast to metals where the knowledge

on their use as EMI shields is fairly matured, experimental EMI SE measurements are needed to assist on the development of CPC materials focused on applications where electromagnetic compatibility, commonly referred to as EMC, is required.

Several SE tests methods have been developed in order to quantify the EMI SE capabilities of materials, some methods such as the ones defined by the *ASTM D4935-10* [5] and *IEEE Std 299-2006* [6] standards are well known, however due to great number of potential test conditions, the electrical nature of the materials to be tested [7], [8], and setup related errors [9]–[11], the EMI SE values for the same material may differ between different test methods. Thus a more robust test setup to measure EMI shielding would be highly desirable.

The EMI shielding test method of enclosures was first introduced by the *MIL-STD-285* standard and later replaced by an improved version, the *IEEE Std 299-2006* standard. Later work such as in [12] suggested improvements for the IEEE standard in order to allow measurements of enclosures with dimensions smaller than 2 m and to define clear fail/pass attenuation limits. In [13] a reverberation chamber technique for measuring the SE of enclosures in the order of 0.1 m cube and smaller is proposed. This sort of input led to the origin of the *IEEE Std 299.1-2013* [14] standard that covers EMI shielding tests of enclosures with dimensions between 0.1 m and 2 m not covered in the IEEE Std 299-2006 standard. However according to [4] in the mode-stirred reverberation method the EMI SE measurements have limited sensitivity to the geometry of the test setup due to the statistical nature of the method. Given that the lower frequencies are related to the reverberation chamber geometry the method can only be safely employed with frequencies typically above 1 GHz.

Whereas the SE test method of enclosures accounts for aspects such as design features on the enclosure the methods used to assist the development of EMI barriers focus on the material itself thus EMI SE test methods for planar material are employed. The waveguide and the transmission line holder are two of the methods used to characterize such materials.

The transmission line method has two distinct approaches to measure the EMI SE, the continuous conductor (CC) and the split conductor (SC) [15]. The CC configuration, based on the ASTM ES7-83 standard withdrawn in 1988, consisted of a 50 Ohms continuous line that could be disassembled to insert an annular testing sample.

The SC approach, defined by the standard ASTM D4935-10, consists of a sample holder, also known as test fixture, transmission line holder, tester and flanged coaxial sample holder, that works as a coaxial transmission line with geometrical characteristics such that the impedance at the connection points and throughout the line is maintained at 50 Ohms, the characteristic impedance. The holder is made of two equal halves with a pair of flanges in the middle to hold the specimens allowing capacitive coupling of energy into insulating materials through displacement current [5]. The gap discontinuity due to the sample thickness is taken in account by using a reference sample that consists of a ring and a disc of the same material. The difference between the measurement without material (*reference specimen*) and with material (*load specimen*) gives the SE that is the result of two distinct shielding mechanisms, the shielding due to reflection and shielding due to absorption.

The ASTM D4935-10 standard covers a frequency range from 30 MHz to 1.5 GHz however various work [16]–[19], have used with more or less success a modified version of this method to perform SE tests in a wider range of frequencies. Other insightful work based also on the ASTM D4935 standard report on a tester developed to operate at frequencies up to 8.0 GHz, [20], [21], and up to 18 GHz [22] reported in a more recent work. These testers are dedicated to the EMI SE measurements of thin films.

Despite the fact that CC and SC methods being widely used the appearance of higher modes inside the sample, due to the reduction of wavelength in conductive materials considered electrically thick, may result in SE errors. This is justified by the fact that at high frequencies the shielding contributions due to absorption is considerable for the case of electrically thick samples [23].

Dual-TEM cells, TEM-t, nested reverberation chambers, and flanged dual-ridged waveguides or H-t cells are examples of other SE test methods used with planar materials.

The purpose of this work is to develop an error-free test setup to assess the shielding effectiveness of conductive polymer composites at frequencies ranging from few kHz up to 3 GHz.

By means of using electromagnetic wave simulations we aim to study different setup designs in order to select and optimize a setup that results in a good compromise between performance (low insertion loss, setup independent frequency response) and easiness of use.

We plan to demonstrate the performance and suitability with a manufactured version of the proposed setup and S-parameters measurements with and without planar samples.

II. S-PARAMETERS

A. SHIELDING EFFECTIVENESS (SE)

In the simplest case an EM wave initially traveling in the free space hits a barrier. Due to difference in impedance between the free space and the barrier, part of the wave initial incident power (P_{IN}) is reflected (P_{RE}), absorbed (P_{AB}), and transmitted (P_{TR}) at different ratios.

$$P_{IN} = P_{RE} + P_{AB} + P_{TR} \tag{1}$$

A vector network analyzer (VNA) measures the phase and magnitude of the scattering parameters (S-parameters) which are characteristic to a device under test (DUT) or similarly to a material under test (MUT). The S-parameters allow to obtain simultaneously the reflected and transmitted power over a given frequency range.

In a two port VNA there are four S-parameters S_{11}, S_{12}, S_{21}, and S_{22}. The $S_{[ij]}$ parameter is the fraction

of signal reflected back to the same port where the signal was initially injected when $i = j$, (S_{11} and S_{22}). The power reflected back to $Port_1$ ($Port_2$) is given by (2).

$$|S_{11}|^2 = \frac{P_{RE}}{P_{IN}}; \quad \left(|S_{22}|^2 = \frac{P_{RE}}{P_{IN}}\right) \tag{2}$$

The $S_{[ij]}$ parameter is the fraction of signal transmitted from $Port_{[i]}$ to $Port_{[j]}$ through the MUT when $i \neq j$, (S_{12} and S_{21}). The total power transmitted from $Port_1$ ($Port_2$) to $Port_2$($Port_1$) is given by (3).

$$|S_{12}|^2 = \frac{P_{TR}}{P_{IN}}; \quad \left(|S_{21}|^2 = \frac{P_{TR}}{P_{IN}}\right) \tag{3}$$

In the case of barriers for electromagnetic compliance internal multiple reflections and other dissipation mechanisms cause part of the signal to be absorbed within the barrier. Using (1) the ratio of absorbed power P_{AB} to the incident power P_{IN} is expressed as follows:

$$\frac{P_{AB}}{P_{IN}} = 1 - \left(|S_{11}|^2 + |S_{21}|^2\right) \tag{4}$$

The evaluation of the SE of a material using the S-parameters takes in account the shielding due to reflection, S_{RE}, and the effective shielding due to absorption, S_{AB}, given in (5) and (6), respectively.

$$S_{RE} = 10.\log_{10}\left(1 - |S_{11}|^2\right)\,[dB] \tag{5}$$

$$S_{AB} = 10.\log_{10}\left(\frac{|S_{12}|^2}{1 - |S_{11}|^2}\right)\,[dB] \tag{6}$$

The total shielding, in dB, is given by the sum of both S_{RE} and S_{AB} contributions:

$$S_{Tot} = S_{RE} + S_{AB}\,[dB] \tag{7}$$

Equation (7) is used to compute the total shielding measured in both cases, with the reference specimen ($S_{Tot-REF}$) and with the load specimen ($S_{Tot-LOAD}$). The SE value is given by subtracting the total shielding measured with the load specimen, $S_{Tot-LOAD}$, from the shielding measured with the reference specimen, $S_{Tot-REF}$, as in (8) yielding a positive value.

$$SE = S_{Tot-REF} - S_{Tot-LOAD}\,[dB] \tag{8}$$

A very high shielding measured with the load specimen will result in a high (positive) SE whereas a very low shielding measured with the load will be almost fully cancelled by the shielding measured with the reference specimen.

B. CHARACTERISTICS OF THE SE TESTER

The performance of the manufactured SE Tester setup was assessed by using a set of parameters, well-known among the microwave community, hereafter presented.

In a lossless network the sum of the signal power entering all the network ports is equal to the sum of signal powers leaving all the network ports, meaning that no power is lost inside the network itself. This is formulated in [24] as follows:

$$\sum_{i=1}^{n} |S_{im}|^2 = 1 \tag{9}$$

For a two port VNA (9) results in two conditions, the lossless network conditions given in (10) and (11). A third condition, the impedance mismatch, is given by (12).

$$|S_{11}|^2 + |S_{12}|^2 = 1 \tag{10}$$

$$|S_{21}|^2 + |S_{22}|^2 = 1 \tag{11}$$

$$|S_{11}| + |S_{22}| = 0 \tag{12}$$

The magnitude of the $|S_{11}|$ ($|S_{22}|$) parameter, known as the reflection coefficient (Γ), $\Gamma = |S_{11}|$, allows to obtain the voltage standing wave ratio ($VSWR$) as follows:

$$VSWR = \frac{1 + \Gamma}{1 - \Gamma}. \tag{13}$$

The insertion-loss (IL) is given as follows:

$$IL = -20 * \log_{10}\left(\left|S_{ij}\right|\right)\ [dB], \quad i \neq j. \tag{14}$$

III. SETUP DESIGN AND VALIDATION

A. SETUP DESIGN CONSIDERATIONS

For the design of the SE test setup we choose the coaxial holder method defined in [5]. This method is preferred due to its simplicity, compactness and the possibility to customize the dimensions of the tester to a desired sample size and the operating frequency range to the higher frequencies available on the VNA.

To obtain the best SE test setup, hereafter referred to as the *SE Tester*, four different setup designs shown schematically in Fig. 1 were initially considered and finite-element methods (FEM) simulations were performed using the electromagnetic (EM) wave simulation software CST STUDIO SUITE®.

Configuration A (Fig. 1 a) is the simplest case where the inner conductor has the same diameter, d = 3.040 mm, as the pin of an APC-7mm connector. In configuration B (Fig. 1 b) the coaxial line is designed using an impedance-matched step representing the transition from the APC-7mm connector to a larger diameter coaxial line. Configuration C (Fig. 1 c) uses a coaxial-conical-coaxial design whereas configuration D (Fig. 1 d) uses 2 locations with a coaxial-spherical-conical transition design. A transmission line similar to the one represented in Fig. 1 a) was implemented by [17] and [18] to operate in a frequency range up to 13.5 GHz. But with no mention of the insertion loss performance of the empty SE Tester.

The small diameter of the inner conductor of a design such as in configuration A with $d = 3.040\ mm$, makes the task of producing and handling samples of this size difficult, and the sample itself may not be representative of the MUT.

The configuration B aims to ease the problem with reduced sample size by increasing the diameter of the inner conductor to $d = 5.00\ mm$. The step transition from the APC-7mm

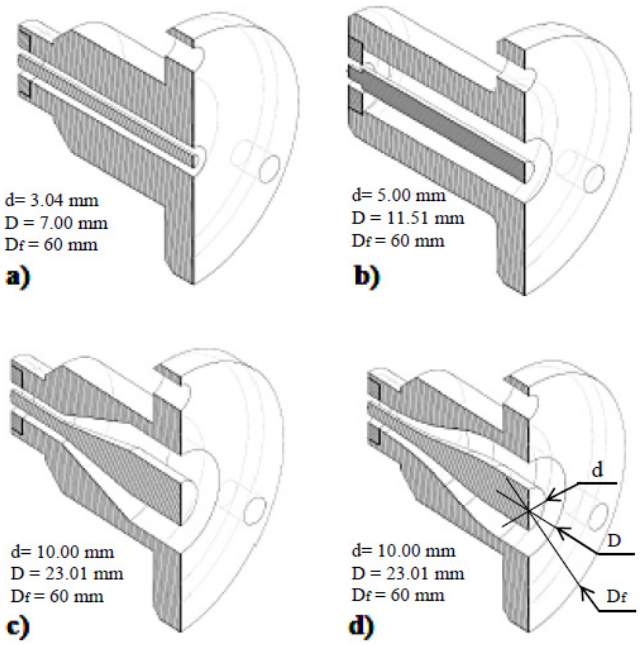

FIGURE 1. 3D CAD of different SE Testers configurations: a) Ideal coaxial line with small diameter inner conductor, b) coaxial line with a step-transition, c) coaxial-conical line, and d) smooth transition transmission line. The dimensions d, D and Df represent the outer diameter of the inner conductor, the inner diameter of the outer conductor and the flange diameter, respectively.

connector to the SE Tester inner conductor takes in account the design principle 1 and 2 defined in [25]. The two principles define that 1) the characteristic impedance needs to be maintained constant along the transmission line and 2) an unavoidable impedance discontinuity needs to be corrected by introducing an individual coplanar compensation as show in [25, Fig. 16].

Configuration C is a transmission line with a coaxial-conical-coaxial design similar to the ASTM D4935-10 standard. This configuration was implemented in [26] through the use of a compensating method [26, Fig. 4] that results in an improved transmission line, comparatively to the ASTM 4539-10 SE Tester, with a input return loss < -20 dB in the 30 MHz - 3 GHz frequency range and no mention of the insertion loss.

The configuration D is the result of combining the aspect of easier sample preparation and handling with the fundamental design principles for precision coaxial components given in [25]. This design which is novel in the context of EMI SE measurements, was inspired by the work reported in [27]–[29] on the development of a ten-way transmission line power combiner. In this configuration a conical section is employed instead of stepped coaxial matched sections to overcome problems with the high electric fields that may originate at sharp edges. In addition a smooth *spherical* transition between the coaxial and conical section, similar to a Klopfenstein taper [30], is implemented to ensure impedance continuity at the transition.

To implement the different configurations with special focus on what seemed to be the best SE Tester design, Fig. 1, d), the dimensions of the inner conductor were defined by the dimensions of the APC-7mm connector on one side and by the diameter of the reference sample inner disc at the flange side. The inner conductor has a $d_1 = 3.040\ mm$ on the side interfacing with the APC-7mm connector, as defined in the Annex D of IEEE Std 287-2007 standard [31], and a $d_2 = 10\ mm$ on the flange side. The original inner conductor of the APC-7mm connector was replaced by embedding it in the design of the SE Tester inner conductor.

The characteristic impedance (Z_0) of a coaxial transmission line is defined as follows:

$$Z_0 = \frac{\eta_0}{2\pi\sqrt{\varepsilon_r}} \ln\left(\frac{D}{d}\right) \ [\Omega]. \tag{15}$$

The variables used in (15) for an air-line are: the free space wave impedance $\eta_0 = 377\Omega$, the relative permittivity of air $\varepsilon_r = 1$, the inner diameter of the outer conductor D, and the outer diameter of the inner conductor d.

Using the transition approach as defined in [25, Fig. 10] and [30] a spline defining the profile, with the transition from d_1 to d_2, of the inner conductor is implemented with MATLAB®. The inner diameter of the outer conductor D is then uniquely defined by solving (15) for D, as in (16), and by computing a new D value for every change in d along the transmission line.

$$D = d.e^{\left(\frac{2\pi Z_0\sqrt{\varepsilon_r}}{\eta_0}\right)} \ [m] \tag{16}$$

B. EM WAVE SIMULATION

The geometry of each configuration was associated with a material from the software database, namely air for the dielectric medium ($\varepsilon = 1.00059$; $\mu = 1.0$), annealed copper ($\sigma = 58e+06$ S/m; $\mu = 1.0$) for the conductors and Polytetrafluoroethylene (PTFE) ($\varepsilon = 2.1$; $\mu = 1.0$) when centering rings are included.

Following the different design concepts presented in Fig. 1 EM wave simulations were performed with frequencies up to 12.0 GHz to evaluate the performance of each configuration. Fig. 2 shows the IL and the VSWR obtained for the different SE Tester configurations. For frequencies below 3.0 GHz configuration A gives an IL < 0.02 dB and an IL < 1.01 dB for higher frequencies.

The high insertion losses observed for configuration B are due to the impedance mismatch at the step transition. For frequencies below 3.0 GHz a maximum IL of 0.92 dB is obtained. The IL value worsens with the frequency increase, as shown in Fig. *2*, a).

Configuration C shows IL < 0.03 dB close to the IL < 0.02 dB value obtained with configuration D for frequencies lower than 3.0 GHz, however resonant peaks in configuration D are more common and the IL value tends to increase with the increase of frequency as shown in the VSWR plot (Fig. *2*, b).

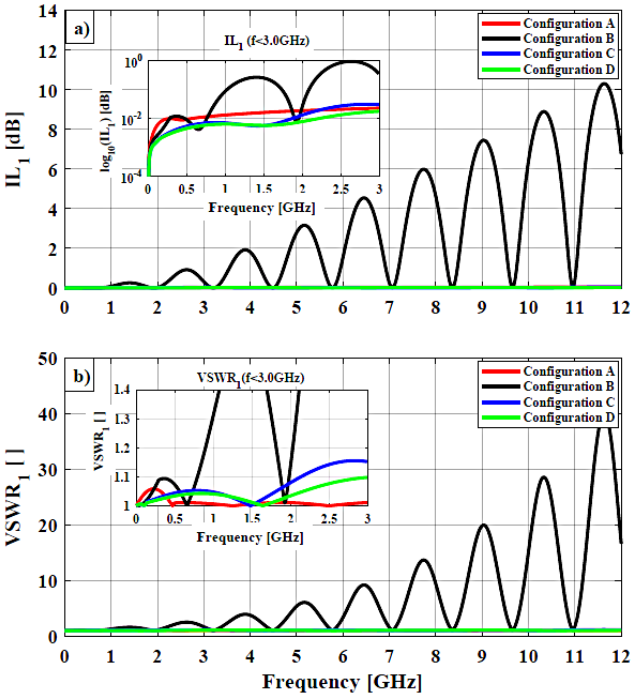

FIGURE 2. Simulated Insertion loss (IL) a) and voltage standing wave ratio (VSWR) b) values obtained with the SE Tester configurations A, B, C, and D.

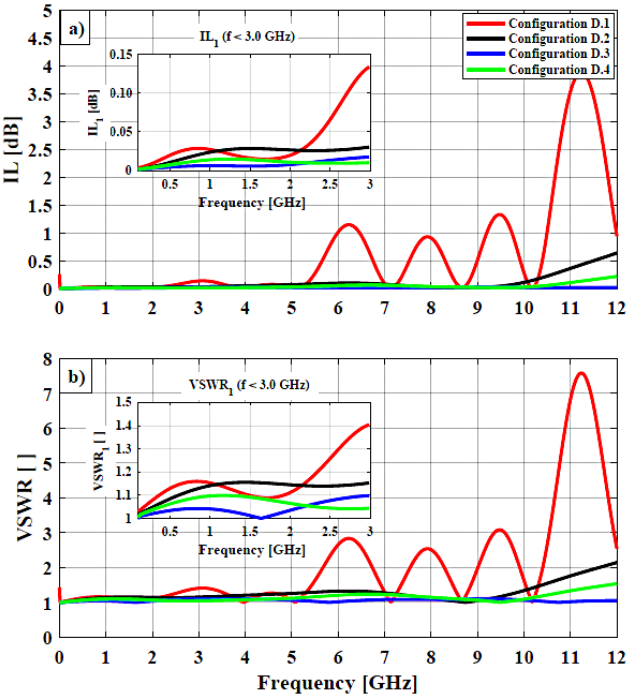

FIGURE 3. Simulated Insertion Loss (IL) a) and Voltage Standing Wave Ratio (VSWR) b) of SE Tester Configuration D.1 (with 4 rings and 4 overcuts), D.2 (2 rings with 2 overcuts), D.3 (no rings or recesses), and D.4 (1 ring without overcut).

According to the simulations configuration D offers the best tradeoff between usability and simulated performance and it is the configuration we selected for further optimization.

C. SETUP OPTIMIZATION

Geometrical features such as centering rings and overcuts were added to the design of configuration D, Fig. 1 d), to assess their impact on the SE Tester performance. Fig. 3 shows the IL and VSWR simulated values obtained for the configuration D.1 (4 rings/4 overcuts), configuration D.2 (2 rings/2 overcuts), configuration D.4 (2 rings/no cuts), and configuration D.3, the original configuration D with no rings nor recesses.

From Fig. 3 a) is possible to see that in configuration D.1 the IL $<$ 0.13 dB up to 3.0 GHz. Configuration D.2 and D.4 are similar, both have a ring to center the inner conductor close to the flange, however configuration D.2 design included an overcut on the outer conductor to fix the centering ring, this resulted in an IL $<$ 0.03 dB compared to IL $<$ 0.01 dB for configuration D.4 at 3.0 GHz. In both cases, the presence of the centering ring, shifted the first near-zero-reflection discontinuity to higher frequencies, namely to 8.7 GHz and 9.5 GHz for configuration D.2 and D.4, respectively.

The VSWR values, shown in Fig. 3 b), for the full simulated frequency range is smaller than 1.2 for configuration D.3 and D.4, however specially for the configuration D.1 the VSWR is substantially aggravated with the increase of frequency. This effect is caused by the overcuts close to the connector side where the conductor's diameter are smaller resulting in higher current density and consequently high electric fields at the sharp edges of the recesses.

Excluding configuration D.3 which is unfeasible in terms of implementation, configuration D.4 is the design that gives the best simulated results and is therefore used to further study possible effects due to varying the gap distance between the SE Tester flanges.

D. GAP-DISTANCE EFFECTS

To assess how the gap-distance, or equivalently sample thickness hereafter referred to as *gap*, affects the EM wave propagation we implemented a script to generate the 2D profiles of SE Tester configuration D.4 with a gap varying from 0.5 mm to 4.0 mm. The 2D contours were then used to create the SE Tester/sample axisymmetric 3D geometries with CST STUDIO SUITE®. EM wave simulations were performed using reference and load specimens for eight different thicknesses and two quasi-EMI transparent materials, Polyimide (PI) ($\varepsilon = 3.5$; $\mu = 1.0$) and PTFE ($\varepsilon = 2.1$; $\mu = 1.0$). The simulated S-parameters values were exported to ASCII files for each of the eight simulations and the SE was computed using (5), (6), (7), and (8) similarly to the procedure for experimental data.

The simulated SE values shown in Fig. 4, for PTFE a), and PI b), are close to zero however at the points where the frequencies of the EM wave matches the resonant frequencies

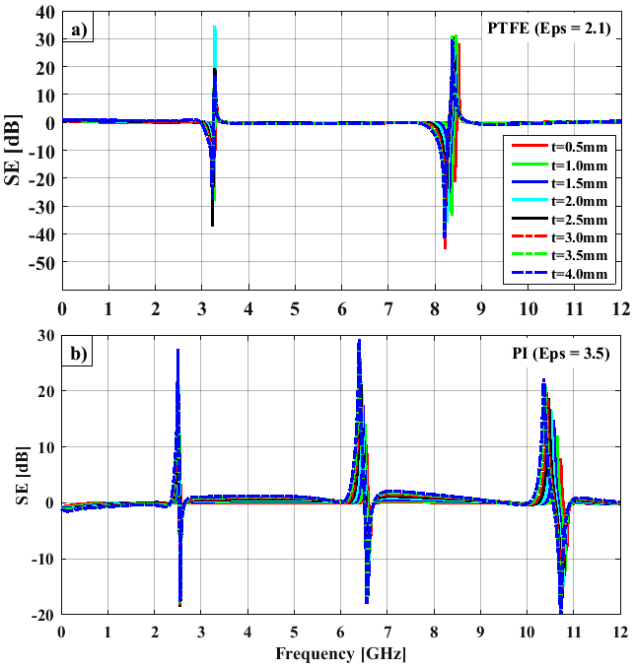

FIGURE 4. Simulated SE values obtained for the SE Tester configuration D.4 with samples of a) PTFE and b) PI materials and of varying thickness.

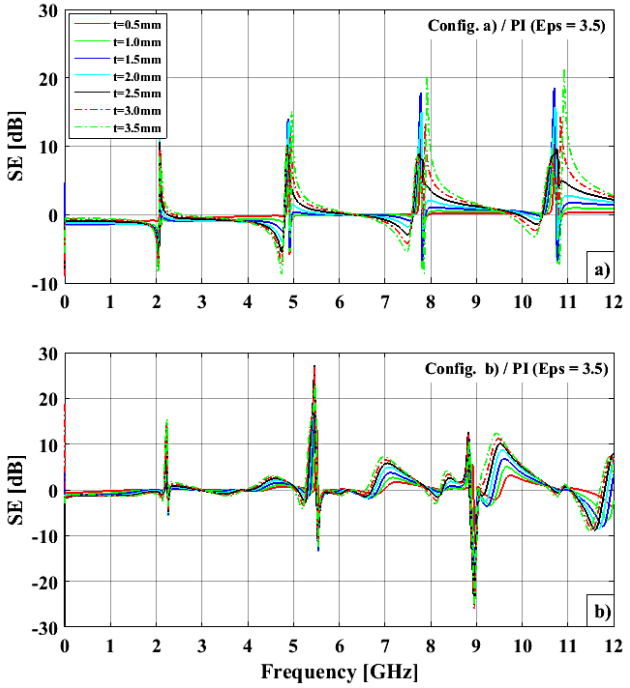

FIGURE 5. SE values obtained from EM wave simulations for a) SE Tester configuration A and b) SE Tester configuration B with PI samples of varying thicknesses.

of the material absorption takes place. A wider gap and higher permittivity value result in a higher anomalous dispersion around the resonance frequency of the material, an effect which becomes more visible with frequency increase.

According to the work reported in [32], at higher relative permittivity values, such as for PI compared to PTFE in our case, the electrical depth in the gap is bigger due to a greater power escape at this location. This explanation could be used to justify the small differences in SE for PTFE and PI at the material non-resonant frequency where the SE values level off.

Resonant frequencies (ω_0) of the material are a material related phenomenon and thus shall be distinguished from setup related resonance frequencies. To evaluate the setup effects together with ω_0 of the MUT, i.e. how the SE Tester setup impacts the SE values, we performed simulations for configuration A and configuration B, two configuration which we expect to influence differently the SE values due to their distinct performances. The material used was PI instead of PTFE due to its slightly higher dielectric constant.

From the simulated SE values, shown in Fig. 5, it is possible to observe that the ω_0 values of PI shift to lower frequencies comparatively to Fig. 4 b). In configuration A (Fig. 5, a) the increase of sample thickness and frequency results in the broadening of the absorption region around ω_0. Despite the fact that configuration A gives the lowest IL values this result seems to indicate that a setup with larger cross section, i.e. larger D and d such as in configuration D.4, is preferred to a design with a small cross section where the EM waves are tightly confined and thus more susceptible to gap effects.

Whereas it is still possible to distinguish the peaks in configuration B, Fig. 5, b), from the ω_0 of PI at around 2 GHz, 5.5 GHZ, and 9 GHz impedance mismatches in this configuration result in localized errors accounted as SE. This effect is aggravated with the increase of both the gap thickness and frequency.

According to the simulations performed we concluded that configuration D.4 produced the best results and is therefore the preferred design for further implementation.

IV. EXPERIMENTAL MEASUREMENTS

A. SETUP CONSTRUCTION

The design of configuration D.4 was used to produce detailed 2D technical drawings for the manufacturing of the final SE Tester. The SE Tester was manufactured with AMPCOLOY® 972 material ($\sigma = 51e + 06$ S/m) using a DMU 60 monoBLOCK® CNC milling machine with a solid carbide tool. A cut view of the 3D CAD and the manufactured SE Tester is shown Fig. 6.

B. SETUP VALIDATION

To perform the S-parameters measurements an Agilent 8753ES VNA, having a 30 kHz to 3 GHz frequency range, was used with two phase-matched 50 Ohms APC-7mm test port cables. To interface with the VNA a Prologix, LLC GPIB-USB controller was used together with a laptop. In order to take data and adjust the VNA settings (output power, stimulus signal start/stop frequency, number of trace points, data format, within others) a script was implemented using the Instrument Control Toolbox in MATLAB®.

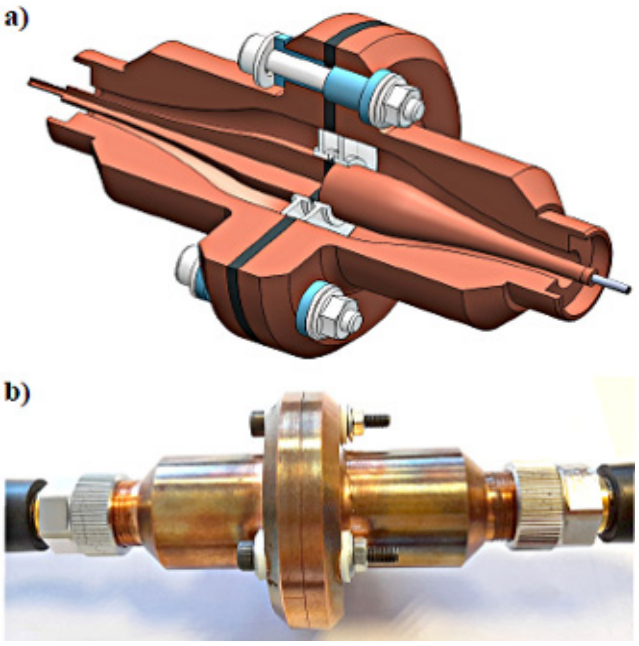

FIGURE 6. 3D CAD design a) and current SE Tester configuration D.4 b) designed with SOLIDWORKS® 3D CAD software.

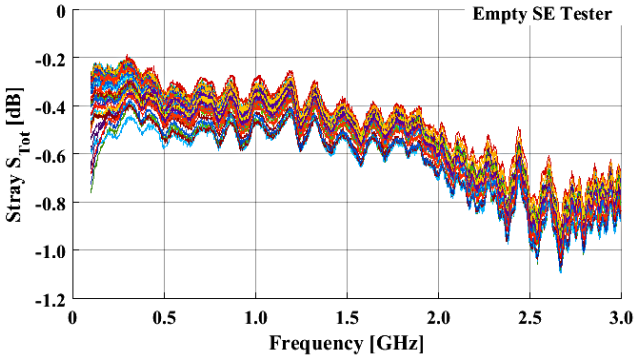

FIGURE 7. Total stray shielding measured fifty times after each unmounting and mounting of the empty SE Tester.

The validation of the newly manufactured SE Tester was done by performing fifty measurements each preceded by the unmounting and mounting of the empty SE Tester. Using (7) we calculated the SE contributions of the empty SE Tester for each test, as shown in Fig. 7. The average total stray shielding for the empty SE Tester is below −1dB, Fig. 8 a), with a standard deviation (STD), Fig. 8 b), smaller than 0.14 dB. For frequencies lower than 1 GHz the STD is greater than that seen for the rest of the frequency range. The small STD values show that the mounting and unmounting process of the SE Tester yields good repeatability. Thus the transmission characteristic of the empty SE Tester is considered flat as a function of frequency with absolute stray shielding contribution of 1 dB for the 30 kHz to 3 GHz frequency range or of $\frac{1}{6}$ dB/decade.

Simulated and measured S-parameters, identified by "(s)" and by "(m)", respectively, obtained with the empty SE

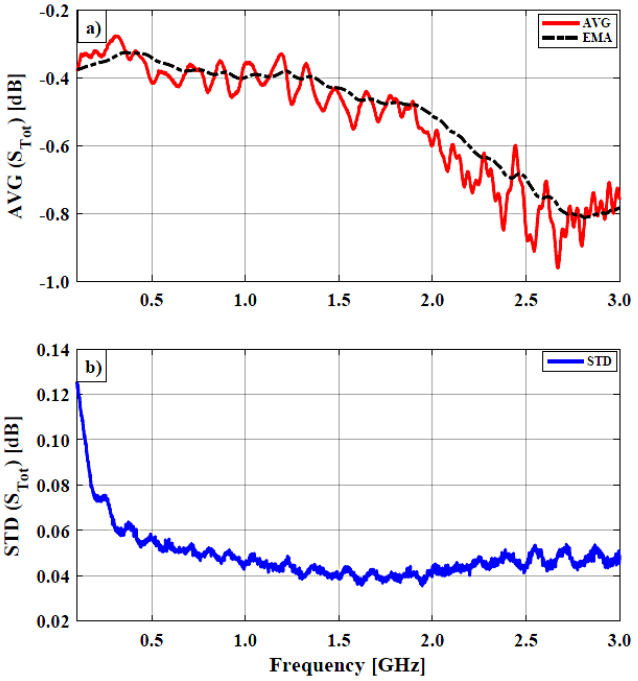

FIGURE 8. Average value of the total stray shielding a) and standard deviation b) obtained with fifty measurements with the empty SE Tester.

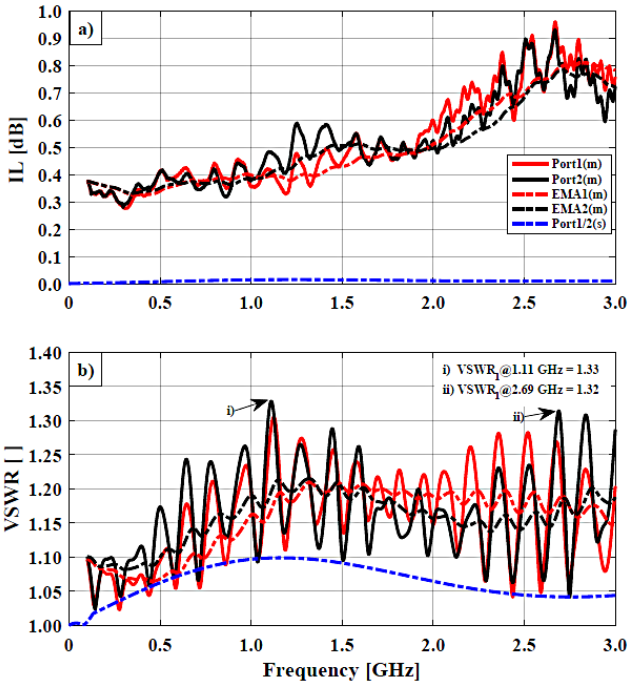

FIGURE 9. Simulated (s) and measured (m) insertion loss a) and voltage standing wave ratio b) obtained with the SE Tester configuration D.4.

Tester configuration D.4 were used to compute the VSWR using (13) and the IL using (14). The suffix 1 and 2 relate to the VNA $Port_1$ and $Port_2$, respectively. The simulated values for $Port_1$ and $Port_2$ are exactly the same since the SE Tester design model is ideal and thus perfectly symmetric.

In Fig. 9 a) the maximum measured IL in *Port1(m)* is 0.961 dB and in *Port2(m)* is 0.932 dB at 2.67 GHz and minimum of 0.279 dB at 298 MHz for both cases. To better represent the trends of the measured values we applied an exponential moving average (EMA1/2) to the IL and VSWR values. The EMA plots give an IL < 0.812 dB for the overall frequency range and an IL < 0.514 dB for frequencies lower than 2.0 GHz.

The maximum VSWR obtained at port 2, Fig. 9 b), is 1.33 and 1.32 at 1.11 GHz and 2.69 GHz, respectively. A VSWR < 1.22 for the whole range is obtained in the EMA plots.

Whereas the simulated IL is in the order of few hundredths of a decibel, 0.015 dB, the actual measured value is on the order of few tenths of a decibel. According to the test port cables datasheet the cables have an IL < 0.5 dB at 2 GHz and IL < 0.9 dB at 6 GHz. Since the measured values include the IL from the cables, cable - SE Tester connection and the SE Tester itself we presume that the IL of the SE Tester alone, as in the simulated case, is smaller than the reported value of 0.812 dB. Nevertheless it is worthwhile to mention that the simulations predicted very well the behavior of the produced SE Tester as shown in Fig. 9 b). At the frequency values where the near-zero-reflections occur, or lowest values computed for VSWR, the measured values intercept the plot Port1/2(s) of the simulated values. In addition the VSWR *EMA*1 *and EMA*2 plots follow a similar trend as in the plot Port1/2(s) obtained with the simulated S-parameters.

We computed the *skin depth* δ using the electrical conductivity of AMPCOLOY® 972 and frequencies within the VNA frequency range, as shown in Fig. 10. A milling process, as the one used to manufacture the SE Tester, results in surface roughness ranging from few tens of micrometer down to few tenths of micrometer in the very best case. The skin depth obtained at 30 kHz, 1.0 GHz and 3.0 GHz is of 288 μm, 1.6 μm and 0.9 μm, respectively. At 3.0 GHz the annealed copper used in the simulations gives a similar δ value of 0.85 μm.

The combined effect of skin depth and surface roughness is a possible explanation for the small ripple-like effect seen in the measured values which intensify when frequency increases, i.e. higher frequencies result in a smaller skin depth and the alternating current becomes more susceptible to the quality of the surface finish of the SE Tester.

Besides the skin effect small localized impedance mismatches seem to be the cause of the two maximum VSWR measured values. In order to evaluate the reciprocity of the SE Tester we computed the average value of S_{12} and S_{21} parameters, as shown in Fig. 11 a).

Contrary to what happens in an ideal two ports reciprocal network, where $S_{12} = S_{21}$, small differences exist between the measured S_{12} and S_{21} values. The highest absolute difference, as shown in Fig. 11 b), of S_{12} and S_{21} ($|S_{12} - S_{21}|$) happens at 1.27 GHz and 2.16 GHz close to the frequencies with the highest VSWR values. These results seem to support the idea that non-reciprocity is caused by localized impedance

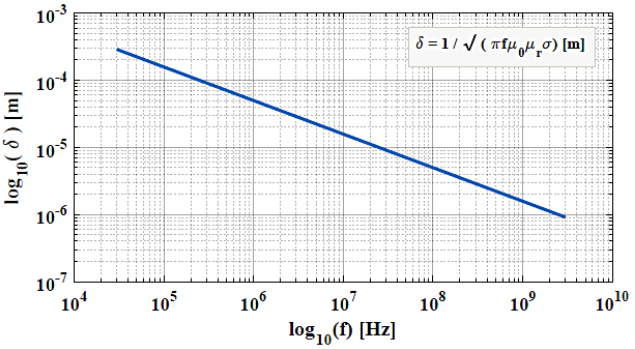

FIGURE 10. Skin depth computed with the AMPCOLOY® 972 properties and frequencies ranging from 30 kHz up to 3.0 GHz.

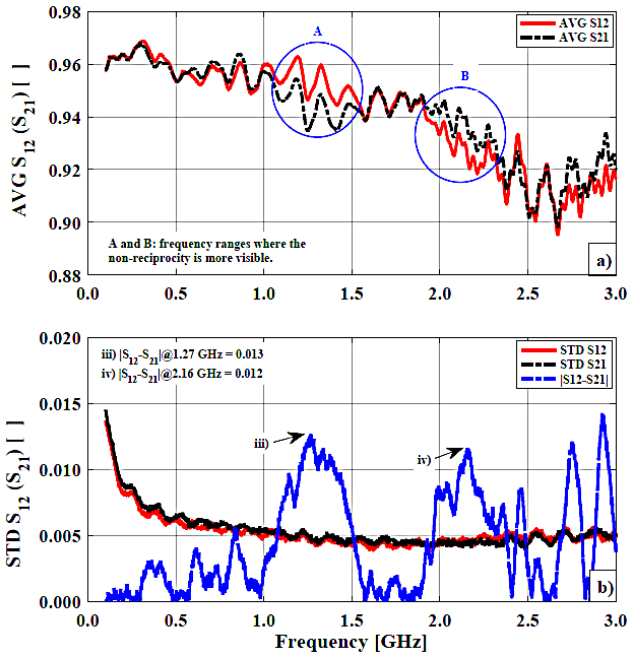

FIGURE 11. Average S12 (S21) S-parameters values obtained with fifty measurements with the empty SE Tester configuration D.4.

mismatches possibly in part due to small discontinuities at the connector - setup transition and small misalignments between the two SE Tester halves. Roughness is very unlikely to be the cause of such localized effects since it affects the whole surface of the tester in the same way.

By applying the lossless network conditions using (10) and (11) the lowest value of 0.82 occurs at 2.67 GHz whereas the highest value of 0.94 occurs at 300 MHz for both cases. The impedance mismatch condition (12) gives the highest values of 0.27, and 0.25 at 1.12 GHz, and at 2.68 GHz, respectively being 0.03 the lowest value at 142 MHz.

The losses in the SE Tester increase for frequencies greater than 2.0 GHz and the frequencies at which the highest impedance mismatches occur support the previous conclusions reached for the VSWR and non-reciprocity results.

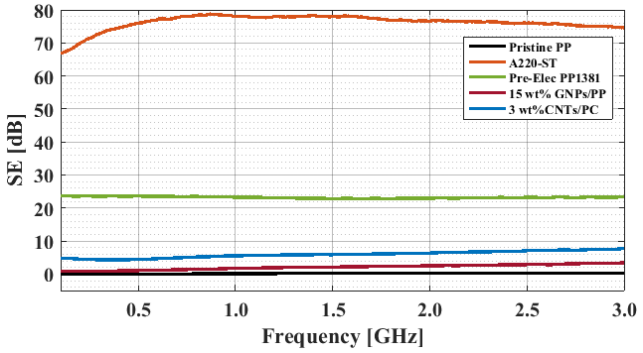

FIGURE 12. EMI SE values measured for 2 mm thick samples produced using conductive polymer composites (CPC) and pristine polymer.

C. SHIELDING EFFECTIVENESS MEASUREMENTS

In order to further assess the performance of the SE Tester we performed EMI SE measurements using five equally thick but electrically very different polymer composites samples produced by injection molding, as it is shown in Fig. 12.

Five different materials were used, namely: Pristine *PP* Adflex X 500 F supplied by LyondellBasell, the *A220-ST* PREMIER^{TM} EMI shielding commercial compound supplied by Chomerics Division Europe (UK), a commercial conductive carbon black concentrate PRE-ELEC® *PP1381* supplied by PREMIX OY (Finland), a less conductive *15 wt% GNPs/PP* concentrate from another supplier and a *3 wt% CNTs/PC* diluted from the PLASTICYL^{TM} PC1501 commercial concentrate supplied by Nanocyl SA. (Belgium). We performed ten measurements for each material, five with the reference and five with the load specimen. The results shown in Fig. *12* are the averaged values obtained for each material.

The thin insulating layer that results at the surfaces of composite samples produced by injection molding may cause additional sample - tester contact impedances that add up to SE value if the tester design is not appropriate [10]. In this scenario the error added to the true SE of the MUT results in an exponential decaying SE plot at lower frequencies due to the increase of the SE by few tens of dB which consequently results in overestimating the shielding properties of the MUT at these frequencies.

In our case the SE plots for the different materials show that the SE Tester is insensitive to the effects abovementioned. The SE obtained for the pristine PP is a flat line at nearly 0 dB as expected. The A220-ST material gives a maximum SE value of 78.1 dB at 1.0 GHz, very close to the 80 dB figure of merit value for this grade, followed by a decrease in SE a trend which is seen in similar grades such as the A240-HT and A230-HT as per the material datasheet. Additionally materials such as the PRE-ELEC® PP1381 show a quasi-frequency independence with an almost SE-frequency linear response up to 3 GHz at a SE value of 23 dB.

In the context of CPC it is worth to mention that the SE value at different frequencies for a given sample is dependent not only on the composite material itself but also on its thermo-mechanical history that impacts the sample and bulk composite morphology, and ultimately the SE response. However a deeper understanding on how such aspects influence the SE-frequency response of the different conductive polymer composites is a subject of future research.

V. SUMMARY

Based on coaxial transmission line principles and the test method defined by the ASTM 4935-10 standard four generic SE test setup designs were proposed and studied with electromagnetic wave simulations.

To the best performing setup small geometrical features were added to bring it closer to a practical setup and new simulations were performed for further optimization.

Additional simulations were performed to study the effects of separating the tester halves on the propagation of electromagnetic waves.

Based on the simulations optimization a setup was manufactured and validated with fifty consecutive unmounting and mounting of the empty SE Tester. S-parameters were measured after each mounting to evaluate the reproducibility of the setup. Additionally five equally thick but electrically different conductive polymer composites planar samples were used to measure their shielding effectiveness.

The optimization resulted in a novel coaxial-spherical-conical smooth transition design with a good performance given by a low insertion loss, high repeatability and a good tradeoff between performance and usability.

VI. CONCLUSIONS

Long-standing, but still sound and very useful, design principles for precision coaxial components in combination with the flexibility of 3D EM simulation software proved to be crucial in defining a reliable setup for EMI shielding effectiveness measurements.

Simple, yet helpful, equations proposed in the literature such as impedance mismatch, lossless network condition and the reciprocity were used, to our knowledge, for the first time within the context of SE testing of planar materials to help in understanding the performance of the SE Tester.

From the simulations we concluded that the sample thickness, sample electrical properties, and the setup design are aspects that all impact the SE results. Interestingly a setup with a small cross section, similar to that of an APC-7mm connector, gives the lowest voltage standing wave ratio when simulated without gaps, however such design is outperformed by a properly designed setup with larger cross section when simulated with the discontinuities imposed by the insertion of a quasi-EMI transparent sample.

We deduced that a setup with a larger cross-section is preferred to a small cross-section setup where the EM waves are extremely confined and thus more susceptible to the unavoidable discontinuity due to the sample thickness.

We achieved a satisfactory averaged insertion loss value lower than 0.812 dB and a standard deviation value of 0.015 with the measured parameters S_{12} and S_{21} for frequencies up

to 3.0 GHz. The most visible impedance mismatches, given by (12), happen at 1.12 GHz and 2.68 GHz. The lossless network conditions given by (10) and (11) result in values lower than 0.9 for frequencies higher than 2.0 GHz.

We established that the mismatches arise most likely due to the SE tester inner-conductor – connector transitions and small misalignments affecting the reciprocity of the setup. The increase of loss with frequency is justified with the skin effect and surface quality.

Performance aspects such as reciprocity and insertion loss could be further improved in future work through the use of finer mechanics aiming high dimensional accuracy, improved surface finish and surface treatments at the expense of high costs which are currently unpractical in the framework of this research.

The SE Tester herein proposed proved to be adequate and a useful test method to gain insight and support future work related to the development of polymer composites for EMI shielding applications.

ACKNOWLEDGMENT

Rosério Valente thanks Prof. Marta Ramos and Prof. Luís Marques from Center of Physics, Dep. of Physics, University of Minho, Portugal, for their suggestions on the setup design validation, Bob Glazer, Product Manager at Amphenol RF, California, USA, for his help within the possible on understanding intricate details of the APC-7mm connector, and Harish Rutti Sales Manager at Chomerics Division Europe, High Wycombe, United Kingdom for providing the free of charge materials used in the injection molding of samples for the SE measurements.

REFERENCES

[1] A. Gupta and R. K. Jha, "A survey of 5G network: Architecture and emerging technologies," *IEEE Access*, vol. 3, pp. 1206–1232, 2015.

[2] A. Zanella, N. Bui, A. Castellani, L. Vangelista, and M. Zorzi, "Internet of Things for smart cities," *IEEE Internet Things J.*, vol. 1, no. 1, pp. 22–32, Feb. 2014.

[3] W. H. Parker, "Electromagnetic interference: A tutorial," in *Proc. IEEE Aerosp. Appl. Conf.*, vol. 3. Aspen, CO, USA, Feb. 1996, pp. 177–186.

[4] A. Junge, J. Wolf, N. Mora, F. Rachidi, and P. Pelissou, "Electromagnetic interference control techniques for spacecraft harness," in *Proc. Int. Symp. Electromagn. Compat. (EMC/Tokyo)*, Tokyo, Japan, May 2014, pp. 840–843.

[5] *Standard Test Method for Measuring the Electromagnetic Shielding Effectiveness of Planar Materials*, Standard ASTM D4935-10, ASTM International, West Conshohocken, PA, USA, 2010. [Online]. Available: http://www.astm.org

[6] *IEEE Standard Method for Measuring the Effectiveness of Electromagnetic Shielding Enclosures*, IEEE Standard 299-2006 (Revision of IEEE Standard 299-1997), Feb. 2007, pp. 1–52.

[7] P. F. Wilson, M. T. Ma, and J. W. Adams, "Techniques for measuring the electromagnetic shielding effectiveness of materials: Part I:—Far field source simulation," *IEEE Trans. Electromagn. Compat.*, vol. EMC-30, no. 3, pp. 239–250, Aug. 1988.

[8] P. F. Wilson and M. T. Ma, "Techniques for measuring the electromagnetic shielding effectiveness of materials: Part II:—Near-field source simulation," *IEEE Trans. Electromagn. Compat.*, vol. EMC-30, no. 3, pp. 251–259, Aug. 1988.

[9] Y. Shan, P. Li, and J. Deng, "Planar material sample fixture characterization and application for EMI shielding effectiveness evaluations," in *Proc. Asia–Pacific Symp. Electromagn. Compat.*, Singapore, May 2012, pp. 181–184.

[10] J. Catrysse, M. Delesie, and W. Steenbakkers, "The influence of the test fixture on shielding effectiveness measurements," *IEEE Trans. Electromagn. Compat.*, vol. 34, no. 3, pp. 348–351, Aug. 1992.

[11] J. A. Catrysse, M. de Goeije, W. Steenbakkers, and L. Anaf, "Correlation between shielding effectiveness measurements and alternative methods for the characterization of shielding materials," *IEEE Trans. Electromagn. Compat.*, vol. 35, no. 4, pp. 440–444, Nov. 1993.

[12] M. Hromádka and Z. Kubík, "Suggestion for changes in shielding effectiveness measuring standard," in *Proc. 4th Int. Youth Conf. Energy (IYCE)*, Siófok, Hungary, 2013, pp. 1–4.

[13] C. L. Holloway, J. Ladbury, J. Coder, G. Koepke, and D. A. Hill, "Measuring the shielding effectiveness of small enclosures/cavities with a reverberation chamber," in *Proc. IEEE Int. Symp. Electromagn. Compat.*, Honolulu, HI, USA, Jul. 2007, pp. 1–5.

[14] *IEEE Standard Method for Measuring the Shielding Effectiveness of Enclosures and Boxes Having all Dimensions Between 0.1 m and 2 m*, IEEE Standard 299.1-2013, Jan. 2014, pp. 1–96.

[15] U. Lundgren, "Characterization of components and materials for EMC barriers," M.S. thesis, Dept. Comput. Sci. Elect. Eng., Luleå Univ. Technol., Luleå, Sweden, 2004.

[16] I. L. Al-Qadi, S. M. Riad, R. Mostaf, and W. Su, "Design and evaluation of a coaxial transmission line fixture to characterize portland cement concrete," *Construction Building Mater.*, vol. 11, no. 3, pp. 163–173, Apr. 1997.

[17] H. Vasquez, L. Espinoza, K. Lozano, H. Foltz, and S. Yang, "Simple device for electromagnetic interference shielding effectiveness measurement," *EMC IEEE EMC Soc. Newslett.*, no. 220, pp. 62–68, 2009. [Online]. Available: http://www.emcs.org/acstrial/newsletters/winter09/pp2.pdf

[18] Y. K. Hong, C. Y. Lee, C. K. Jeong, D. E. Lee, K. Kim, and J. Joo, "Method and apparatus to measure electromagnetic interference shielding efficiency and its shielding characteristics in broadband frequency ranges," *Rev. Sci. Instrum.*, vol. 74, no. 2, pp. 1098–1102, Jan. 2003.

[19] C. Chen and Y. Sang, "The development of novel coaxial tester on electromagnetic shielding effectiveness measurement," in *Proc. IEEE 6th Int. Symp. Microw., Antenna, Propag., EMC Technol. (MAPE)*, Shanghai, China, Oct. 2015, pp. 506–510.

[20] A. Tamburrano and M. S. Sarto, "Electromagnetic characterization of innovative shielding materials in the frequency range up to 8 gigahertz," in *Proc. Int. Symp. Electromagn. Compat.*, vol. 2. Aug. 2004, pp. 551–556.

[21] M. S. Sarto and A. Tamburrano, "Innovative test method for the shielding effectiveness measurement of conductive thin films in a wide frequency range," *IEEE Trans. Electromagn. Compat.*, vol. 48, no. 2, pp. 331–341, May 2006.

[22] A. Tamburrano, D. Desideri, A. Maschio, and M. S. Sarto, "Coaxial waveguide methods for shielding effectiveness measurement of planar materials Up to 18 GHz," *IEEE Trans. Electromagn. Compat.*, vol. 56, no. 6, pp. 1386–1395, Dec. 2014.

[23] M. Badic and M.-J. Marinescu, "The failure of coaxial TEM cells ASTM standards methods in H.F. range," in *Proc. IEEE Int. Symp. Electromagn. Compat. (EMC)*, vol. 1. Minneapolis, MN, USA, Aug. 2002, pp. 29–34.

[24] C. Poole and I. Darwazeh, "S-parameters," in *Microwave Active Circuit Analysis and Design*, 1st ed. Amsterdam, The Netherlands: Academic, 2016, pp. 168–204.

[25] T. E. MacKenzie and A. E. Sanderson, "Some fundamental design principles for the development of precision coaxial standards and components," *IEEE Trans. Microw. Theory Techn.*, vol. MTT-14, no. 1, pp. 29–39, Jan. 1966.

[26] C. C. Chen and F. M. Lu, "A compensated flanged coaxial tester for shielding effectiveness measurement," in *Proc. IEEE Int. Conf. Microw. Millim. Wave Technol. (ICMMT)*, vol. 2. Shenzhen, China, May 2012, pp. 1–3.

[27] P. W. Van der Walt, "A novel matched conical line to coaxial line transition," in *Proc. South African Symp. Commun. Signal Process. (COMSIG)*, Rondebosch, South Africa, Sep. 1998, pp. 431–434.

[28] D. I. L. D. Villiers, P. W. V. D. Walt, and P. Meyer, "Design of a ten-way conical transmission line power combiner," *IEEE Trans. Microw. Theory Techn.*, vol. 55, no. 2, pp. 302–308, Feb. 2007.

[29] D. I. L. D. Villiers, P. W. V. D. Walt, and P. Meyer, "Design of conical transmission line power combiners using tapered line matching sections," *IEEE Trans. Microw. Theory Techn.*, vol. 56, no. 6, pp. 1478–1484, Jun. 2008.

[30] R. W. Klopfenstein, "A transmission line taper of improved design," *Proc. IRE*, vol. 44, no. 1, pp. 31–35, Jan. 1956.

[31] *IEEE Standard for Precision Coaxial Connectors (DC to 110 GHz)*, IEEE Standard 287-2007 (Revision of IEEE Standard 287-1968), Sep. 2007, pp. 1–142.

[32] A. C. Marvin, L. Dawson, I. D. Flintoft, and J. F. Dawson, "A method for the measurement of shielding effectiveness of planar samples requiring no sample edge preparation or contact," *IEEE Trans. Electromagn. Compat.*, vol. 51, no. 2, pp. 255–262, May 2009.

ROSÉRIO VALENTE received the M.Sc. degree in mechanical engineering from the University of Aveiro, Portugal, in 2011. During his M.Sc. studies, he took part on a two years exchange program at the University of Science and Technology of Krakow, Poland. His thesis was done on the computer vision–stereo vision systems (thesis: 3-D Points Recover from Stereo Video Sequences Based on Open CV 2.1 Libraries).

From 2012 to 2015, he was with the GSI Center for Heavy Ion Research GmbH, Darmstadt and with the Helmholtz Institute Mainz, Germany, as part of a group of engineers and physicists working on the research and development of a particle physics detector aiming the study of antiproton–proton collisions.

Mr. Valente received a European Union's Marie-Skłodowska-Curie research grant to work on the development of conductive polymers nanocomposites in 2015. Under this grant, he is currently working with Promolding B.V., The Hague, and with the Novel Aerospace Materials Group, Delft University of Technology, Delft, The Netherlands, toward the fulfillment of his Ph.D. degree.

His research interests include the processing of carbon-based polymer nanocomposites, electromagnetic interference shielding, electrostatic discharge, dielectric spectroscopy, and other characterization techniques, such as electron microscopy, X-ray tomography, and rheology.

CHRIS DE RUIJTER received the M.Sc. degree in chemical engineering from the Delft University of Technology in the field of polymer science, in 2001, and the Ph.D. degree in self-reinforcement of liquid crystalline block copolymer materials from the Chemical Engineering Department, Delft University of Technology, in 2006. His M.Sc. thesis consisted of the development of EMI shielding compounds (polymer matrix, copper fibers, and a low melting solder alloy).

From 2006 to 2008, he was a Post-Doctoral Associate on a project related to the development of ester-based resins for aramid ballistic composites at the Faculty of Aerospace Engineering, Delft University of Technology, where he was a Post-Doctoral Associate and a Project Manager with the Adhesion Institute from 2008 to 2011.

Since 2011, he has been with Promolding B.V., The Hague, The Netherlands, as a Senior Researcher. In this position, he has been involved on several research and development projects related to electrically conductive CNTs and graphite-based polymer nanocomposites.

DANIEL VLASVELD received the M.Sc. degree in polymer science from the Faculty of Chemical Technology, University of Twente, The Netherlands, in 2000, and the Ph.D. degree in layered silicate nanocomposites and their use as fiber composite matrix material from the Chemical Technology Department, Delft University of Technology in 2004 (thesis: fibre reinforced polymer nanocomposites).

From 2004 to 2006, he was involved in a post-doctoral project about carbon nanotube reinforced LCP (PPTA) fibers.

Since 2006, he has been with Promolding B.V., The Hague, The Netherlands, first as a Senior Polymer Researcher and currently as a Research and Development Manager. In this position, he has involved in several research and development projects involving electrically conductive CNTs and graphite-based nanocomposites.

SYBRAND VAN DER ZWAAG received the M.Sc. degree from the Dutch Nuclear Research Centre, in 1978, and the Ph.D. degree in 1981. He then joined the Cavendish Laboratory, Cambridge University, U.K., and studied the impact damage in glass and infrared transparent ceramics due to supersonic impact with rain drops. As a post-doc, he studied the relaxation kinetics in amorphous metals (metallic glasses). In 1983, he joined Akzo Corporate Research Laboratories and extensively involved in the structure-property relations in aramid and other high performance fibres as well as new fibre spinning technologies. In 1992, he was appointed as a Full Professor in the chair Microstructural Control in Metals and in 2003 as a Full Professor in the chair Novel Aerospace Materials, both at TU Delft, The Netherlands. He is recognized as one of the founding fathers of the Netherlands Institute for Metals Research (now M2i).

He is the Director of the Delft Centre for Materials and the Chairman of the National IOP Program on Self-Healing Materials. He has published over 480 ISI publications and supervised 48 Ph.D. students.

Prof. van der Zwaag is a member of the Royal Dutch Society for Sciences and a fellow of the (British) Institute of Materials, Minerals and Mining. In 2012, he was granted the honorary title Distinguished Professor by the Board of the Delft University of Technology for his efforts to strengthen the collaboration between the university and industry in the field of materials science. Until 2016, he was the Scientific Director of the Dutch Polymer Institute. In 2017, he received an honorary Ph.D. degree from the University of Mons, Belgium.

His research interests are in the field of micro-structure property relations for novel materials. Within this field, he focuses on the computational design of novel high performance metals, the development of self-healing (polymeric, metallic, and ceramic) materials, as well as the development of novel functional composites.

PIM GROEN received a degree in solid-state chemistry working on areas related to crystal structures of perovskites from Leiden University, The Netherlands, in 1987. He then joined Philips Research, Eindhoven, The Netherlands, where he was involved in inorganic materials for electronic applications and later in Philips Forschung, Aachen, Germany, involved in electronics ceramics, including piezoelectric ceramics.

He received the Ph.D. degree in ceramic superconductors, in 1990. In 2002, by the time Philips stopped its activities in the field of passive components, he joined Morgan Electroceramics as a Research and Development Manager, where he was responsible for the development of several projects involving the implementation of piezo-based technology into commercial products. Within others, he led a project on a new production line for the making of multilayer piezoelectric actuators.

Prof. Groen held the head position of the Materials Performance Group, TNO Science and Industry, from 2008 to 2011. Since 2011, he has been a Program Manager with the Holst Centre, The Netherlands, for the programs Large Area Printing and Printed Conductive Structures. In 2009, in parallel to his other activities, he joined the Novel Aerospace Materials Group as a Visiting Scientist starting new activities in the field of smart materials and sensors. Since 2012, he has been a full-time Professor with the Faculty of Aerospace Engineering, Delft University of Technology, The Netherlands, on the chair SMART Materials in parallel to his work at the Holst Centre.

His research interests are on the fields of novel concepts for piezoelectric composites in sensor devices and energy harvesting with special focus on the areas of structural health monitoring applications in the aviation industry. Other research interests are related to novel piezo plastics and flexible OLEDs materials that envision to revolutionize product interface design by means of integrating luminescence and touch.